Rigorous Coupled-Wave-Theory Analysis of Dipole Scattering from a Three-Dimensional, Inhomogeneous, Spherical Dielectric, and Permeable System

John M. Jarem, *Senior Member, IEEE*

***Abstract*—This paper presents a rigorous coupled-wave-theory analysis (RCWT) of the electromagnetic (EM) radiation, which occurs when a centered electric dipole excites power and energy in a general three-dimensional (3-D) inhomogeneous spherical system. The formulation of this paper consists of a multilayer state-variable (SV) analysis of Maxwell's equations in spherical coordinates (the SV analysis used transverse-to-r spherical EM-field components), as well as a presentation of the EM fields which exist in the interior and exterior regions (which bound the inhomogeneous spherical system). A detailed description of the matrix processing which is involved with finding the final EM fields of the overall system is given. Three numerical examples of the RCWT method are studied. The first example presents EM scattering when a centered dipole radiates through a uniform material shell. In this example, numerical results of the RCWT algorithm are compared with numerical results as obtained by a Bessel-function matching algorithm, and excellent agreement was found between the two methods. The second example presents centered dipole radiation when the spherical system is a dielectric shell, which is inhomogeneous in the (θ, φ) directions, and the third example presents centered dipole radiation when the spherical system is inhomogeneous in the (r, θ, φ) directions. Several examples and plots of the power diffracted into higher order modes by the inhomogeneity profiles are given. As the thickness of the inhomogeneous dielectric shell is increased, it is observed that, through diffraction, power is increasingly depleted from lower order modes into higher modes. The depletion of power from lower to higher order spherical modes with increasing shell thickness is noted to be very similar to the variation of diffraction-order power efficiency, which is observed when the layer thickness of a planar transmission diffraction grating is increased.**

***Index Terms*—Diffraction, inhomogeneious, rigorous coupled-wave theory, 3-D scattering.**

I. Introduction

An important and well-known problem in electromagnetic (EM) theory is the problem of determining the scattering that occurs when an EM wave is incident on a circular-cylindrical or spherical object. These problems have been extensively studied in the cases where: 1) the EM incident wave is an oblique or nonoblique plane wave; 2) the incident EM wave has been generated by a line source or dipole source; and 3) the circular or spherical object is a dielectric-coated metallic object [1]–[5]. Concerning circular-cylindrical systems, the problem of determining plane-wave and line-source scattering from eccentric circular dielectric systems (circular dielectric cylinders of varying dielectric value whose axes are not centered on a single line) has also been studied. Recently, a complete solution to this problem has been obtained in [6], which also gives a complete literature survey of scattering from eccentric and centered circular-cylindrical dielectric systems. Wu [7], [8] studies the problem of plane-wave scattering from circular, homogeneous, anisotropic, dielectric cylindrical-shell systems. Concerning scattering from spherical systems, Ren [9] studies scattering from anisotropic homogeneous spherical systems and also studies Greens' functions associated with anisotropic homogeneous spherical systems. Ren [9] gives a very complete literature survey of scattering from isotropic and anisotropic spherical systems.

A problem concerning circular-cylindrical object scattering, which has further received a great deal of attention, is the problem of determining the scattering and radiation that occurs when the circular-cylindrical dielectric system contains a region whose permittivity is inhomogeneous and periodic in the φ azimuthal direction [10]–[12]. The solution of this problem is of great interest in cylindrical-aperture antenna theory [10] because of the fact that radial and azimuthal dielectric loading in front of a cylindrical-aperture antenna can greatly alter and, therefore, possibly enhance the radiation characteristics of the cylindrical-aperture antenna. Elsherbeni and Hamid [10] study EM transverse-magnetic (TM [electric field parallel to the cylinder axis]), scattering from the inhomogeneous radial dielectric-shell permittivity profile $\varepsilon(\rho, \phi) = \varepsilon_a(\rho_0/\rho)^2[\eta - \delta \cos(2\varphi)]$ where ε_a, ρ_0, η, and δ are constants defined in [10], and ρ and φ are cylindrical coordinates. Homogeneous space occupies the interior and exterior region to the dielectric shell, and the shell is assumed to be homogeneous and infinite in the z-axial direction. The method of solution used by Elsherbeni and Hamid [10] consists of: 1) solving Maxwell's equations in Regions 1 and 3, surrounding the dielectric shell in terms of Bessel functions; 2) solving the ρ and φ inhomogeneous wave equation in Region 2 in terms of Mathieu functions; and 3) matching boundary conditions at Region–1 and Region–3 interfaces to

Manuscript received August 13, 1996; revised April 25, 1997.

The author is with the Electrical and Computer Engineering Department, University of Alabama at Huntsville, Huntsville, AL 35899 USA.

Publisher Item Identifier S 0018-9480(97)05374-X.

determine all the unknown constants of the system. In [12], Elsherbeni and Tew again study the case of TM scattering from a dielectric cylinder, but they extend their analysis to dielectric permittivity profiles where $\varepsilon(\rho, \varphi) = (\rho/\rho_0)^2[\eta - \delta \cos(m\varphi)]$.

Concerning the problem of EM scattering from inhomogeneous-material systems, in a recent paper [13], the author generalized the work of [10]–[12] and presented an EM cyclindrical-solution algorithm to analyze radiation and scattering from an isotropic [13] dielectric cylinder system which has an arbitrary radial and azimuthal $\varepsilon(\rho, \varphi)$ profile rather than the $\varepsilon(\rho, \varphi)$ profile used by [10]—[12]. The solution profile in [13] was based on a recently developed EM planar-diffraction grating algorithm called rigorous coupled-wave theory (RCWT) [14]–[20]. The author [13] extended and generalized the work of Elsherbeni *et al.* [10]–[12] and Wu [7], [8] and extended the RCWT planar diffraction algorithm [14]–[20] to handle the analysis of isotropic inhomogeneous dielectric cylinders [13]. The algorithm of [13] studied the case when the electric field is polarized parallel to the cylindrical-material axis (TM case).

Concerning the problem of EM scattering from inhomogeneous-material spherical systems, this author has submitted a letter [21] describing how the RCWT algorithm can be applied to the analysis of radiation and scattering from a spherical inhomogeneous object. The letter [21] presented the basic spherical equations necessary to analyze an arbitrary three-dimensional (3-D) inhomogeneous scatterer by the RCWT method, and also presented a simple example of dipole radiation from an inhomogeneous dielectric object, which was azimuthally homogeneous (varied in the θ direction but had no dependence in the φ direction). The spherical RCWT analysis of this paper will extend the results of [21] in the following ways. First, the analysis of this paper will study examples where the inhomogeneous scatterer has an inhomogeneous permittivity and permeability profile, which, in addition to varying arbitrarily in the radial direction, also varies arbitrarily in the θ and φ directions. In [21], the inhomogeneity variation was only in the θ direction. This case is much more challenging numerically than [21], because matrix equations for all orders of m and n must be solved rather than a matrix equation for just $m = 0$ and all n. The second way that the results of [21] are extended in this paper is that the basic spherical state-variable (SV) equations and the interior–exterior Bessel-function equation of [21] will be modified to the general case when the inhomogeneous scatterer and EM-source excitation is periodic in the φ coordinate over a region $2\pi/\kappa$, where κ is an integer ($\kappa = 1, 2, 3, \cdots$) rather than being periodic over just 2π, as was presented in [21]. This is particularly useful as only a centered-line excitation is considered in this paper. The third way that the results of [21] are extended is that full radiated-power results for radiation from higher order m and n spherical Bessel–Legendre modes are given, whereas in [21], power results were given only for $m = 0$ modes.

This paper will be concerned with determining the EM fields that result when a centered electric dipole radiates inside a 3-D inhomogeneous-material system (see Fig. 1). This problem may be viewed as either a material shielded-antenna source problem or may be viewed as a material microwave-cavity problem, where the material cavity is formed from the inhomogeneous dielectric and permeable material which surrounds the electric-dipole source.

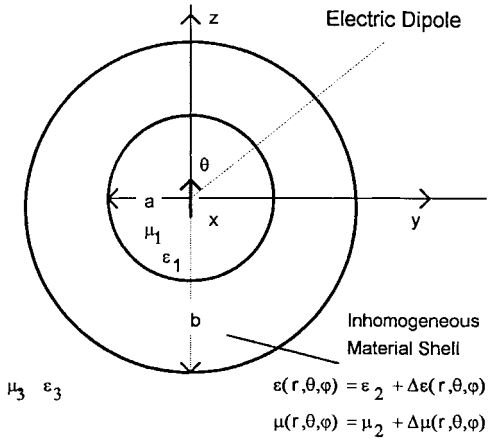

Fig. 1. Geometry of the 3-D inhomogeneous spherical system.

II. Rigorous Coupled-Wave-Theory Formulation

This section will be concerned with putting Maxwell's equations in spherical coordinates into a form for which the RCWT formulation can be implemented. The spherical system shown in Fig. 1 is considered here. All coordinates will be assumed normalized as $r = k_0\tilde{r}$, $a = k_0\tilde{a}$, etc., where $r = k_0\tilde{r}$, $k_0 = 2\pi/\lambda$, λ is the free-space wavelength in meters. In this figure, Region 1 ($0 \le r \le a$) is assumed to be a uniform material with the relative permittivity ε_1 and relative permeability μ_1, Region 3 ($b \le r$) is assumed to be a uniform material with the relative permittivity ε_3 and relative permeability μ_3, and Region 2 with $v = \cos(\theta)$, is assumed to have an arbitrary inhomogeneous lossy relative permittivity $\varepsilon(r, v, \varphi)$ and is assumed to have an inhomogeneous lossy relative permeability $\mu(r, v, \varphi)$. For generality, one assumes that EM radiation may impinge on the 3-D object from Region 3 (e.g., a plane wave) or from Region 1 (e.g., a dipole source). Maxwell's equations of Region 2 will now be put into SV form. If $\varepsilon(r, v, \varphi)$ and $\mu(r, v, \varphi)$ are substituted into the Maxwell's curl equations of Region 2, and the two Maxwell curl equations are expanded into their r-, θ-, and φ-field components, one finds that the longitudinal radial electric- and magnetic-field components may be expressed in terms of the transverse θ, φ electric- and magnetic-field components as

$$E_r = -\frac{1}{j\varepsilon(r, v, \varphi)r^2}\left[\frac{\partial U_\varphi}{\partial v} + \frac{1}{\gamma}\frac{\partial U_\theta}{\partial \varphi}\right]$$
$$H_r = \frac{1}{j\mu(r, v, \varphi)r^2}\left[\frac{\partial S_\varphi}{\partial v} + \frac{1}{\gamma}\frac{\partial S_\theta}{\partial \varphi}\right] \tag{1}$$

where $\gamma = (1 - v^2)^{1/2}$, $S_\theta = r E_\theta$, $S_\varphi = r \sin\theta E_\varphi$, $U_\theta = \eta_0 r H_\theta$, $U_\varphi = \eta_0 r \sin\theta H_\varphi$, and $\eta_0 = \sqrt{\mu_0/\varepsilon_0} = 377\ \Omega$. Substituting these equations into the remaining Maxwell curl

equations, one finds

$$\frac{\partial S_\theta}{\partial r} = j\left[\frac{-\gamma}{r^2}\frac{\partial}{\partial v}\frac{1}{\varepsilon(r, v, \varphi)\gamma}\frac{\partial}{\partial \varphi}\right]U_\theta + j\left[-\frac{\mu(r, v, \varphi)}{\gamma} - \frac{\gamma}{r^2}\frac{\partial}{\partial v}\frac{1}{\varepsilon(r, v, \varphi)}\frac{\partial}{\partial v}\right]U_\varphi \quad (2)$$

$$\frac{\partial S_\varphi}{\partial r} = j\left[\mu(r, v, \varphi)\gamma + \frac{1}{r^2\gamma}\frac{\partial}{\partial \varphi}\frac{1}{\varepsilon(r, v, \varphi)}\frac{\partial}{\partial \varphi}\right]U_\theta + j\left[\frac{1}{r^2}\frac{\partial}{\partial \varphi}\frac{1}{\varepsilon(r, v, \varphi)}\frac{\partial}{\partial v}\right]U_\varphi \quad (3)$$

$$\frac{\partial U_\theta}{\partial r} = j\left[\frac{\gamma}{r^2}\frac{\partial}{\partial v}\frac{1}{\mu(r, v, \varphi)\gamma}\frac{\partial}{\partial \varphi}\right]S_\theta + j\left[\frac{\varepsilon(r, v, \varphi)}{\gamma} + \frac{\gamma}{r^2}\frac{\partial}{\partial v}\frac{1}{\mu(r, v, \varphi)}\frac{\partial}{\partial v}\right]S_\varphi \quad (4)$$

$$\frac{\partial U_\varphi}{\partial r} = j\left[-\varepsilon(r, v, \varphi)\gamma - \frac{1}{r^2\gamma}\frac{\partial}{\partial \varphi}\frac{1}{\mu(r, v, \varphi)}\frac{\partial}{\partial \varphi}\right]S_\theta + j\left[\frac{-1}{r^2}\frac{\partial}{\partial \varphi}\frac{1}{\mu(r, v, \varphi)}\frac{\partial}{\partial v}\right]S_\varphi. \quad (5)$$

The concern will now be with developing a multilayer RCWT analysis that can be used to solve (2)–(5) in Region 2. To proceed, one divides Region 2, $a \le r \le b$, into L thin layers of width d_ℓ, where $b - a = \sum_{\ell=1}^{L} d_\ell$. One assumes that each layer has been made thin enough so that all inhomogeneous functions in the radial coordinate r on the right-hand side (RHS) of (2)–(5) may be considered constant in the thin-shell region and may be approximated by the midpoint value of r in the thin layer. In each thin spherical shell, it is convenient to introduce the local coordinates $s_1 = r - b$ for $b - d_1 \le r \le b$, $s_2 = r - (b - d_1)$ for $b - d_1 - d_2 \le r \le b - d_1, \cdots$. These local coordinates will be used to express the final SV equations in each cylindrical shell. In the ℓth thin-shell layer, (2)–(5) are put in SV form in the local coordinates s_ℓ by expanding all field variables and inhomogeneous factors $\varepsilon(r_\ell^{\text{mid}}, v, \varphi)$, $\gamma(v)$, $1/\mu(r_\ell^{\text{mid}}, v, \varphi)$, $\cdots$ (these functions are assumed sampled at the ℓth radial midpoint r_ℓ^{mid}) in a two-dimensional (2-D) exponential Fourier series, collecting terms together which have the same exponential coefficient factors, and forming a set of first-order differential equations for the mode amplitudes $S_{\theta im}^{(\ell)}$, $S_{\varphi im}^{(\ell)}$, $U_{\theta im}^{(\ell)}$, $U_{\varphi im}^{(\ell)}$. The mode amplitude expansion for $S_\theta^{(\ell)}(s_\ell, \theta, \varphi)$, for example, is given by $S_\theta^{(\ell)}(s_\ell, \theta, \varphi) = \sum_{i,m} S_{\theta im}^{(\ell)}(s_\ell) \exp[j(i\pi v + m\kappa\varphi)]$, where $-\Lambda_\varphi/2 \le \varphi \le \Lambda_\varphi/2$, $-1 \le v \le 1$, $\kappa = 2\pi/\Lambda_\varphi = 1, 2, 3, \cdots$, may be called the azimuthal-grating wave vector and Λ_φ may be called the azimuthal-grating period. The matrix for a general inhomogeneous factor, say $\varepsilon(r_\ell^{\text{mid}}, v, \varphi)$, for example, is

$$\underline{\underline{\varepsilon^{(\ell)}}} = [\underline{\underline{\varepsilon^{(\ell)}}}_{(i,m),(i',m')}] = [\breve{\varepsilon}_{i-i', m-m'}]$$

where

$$\breve{\varepsilon}_{i-i', m-m'}$$

are the 2-D Fourier coefficients of $\varepsilon(r_\ell^{\text{mid}}, v, \varphi)$ and

$$\underline{\underline{\varepsilon^{(\ell)}}}_{(i,m),(i',m')}$$

represents a typical matrix element of the overall matrix $\underline{\underline{\varepsilon^{(\ell)}}}$ {note that (i, m) is an ordered pair representing a single integer in the $\underline{\underline{\varepsilon^{(\ell)}}}$ matrix [same for (i', m')]. The matrices for the differential operators $\partial/\partial v$ and $\partial/\partial\varphi$ are given by the diagonal matrices, respectively,

$$\underline{\underline{D_v}} = [ji\pi\delta_{i,i'}\delta_{m,m'}]$$
$$\underline{\underline{D_\varphi}} = [jm\kappa\delta_{i,i'}\delta_{m,m'}]$$

where $\delta_{i,i'}$ is the Kronecker delta, and the matrices describing the modal field amplitudes are given by column matrices e.g., $\underline{S_\theta^{(\ell)}} = [S_{\theta(i,m)}^{(\ell)}]^t$ (t is transpose). Replacing each inhomogeneous factor, derivative operator, and field amplitude by the appropriate matrix, the overall system SV matrix may be found. The first right-hand term of (2), for example, is given by

$$-(j/r_\ell^{mid^2})(\underline{\underline{\gamma}}\{\underline{\underline{D_v}}[\underline{\underline{K_{1/\varepsilon\gamma}^{(\ell)}}}(\underline{\underline{D_\varphi}}\,\underline{U_\theta})]\}) = \underline{\underline{A}}_{1,3}^{(\ell)}\underline{U_\theta}$$

where $\underline{\underline{\gamma}}$ and $\underline{\underline{K_{1/\varepsilon\gamma}^{(\ell)}}}$ matrices represent the factors $\gamma(v)$ and $1/[\varepsilon(r_\ell^{\text{mid}}, v, \varphi)\gamma(v)]$, respectively. The matrix $\underline{\underline{A}}_{1,3}^{(\ell)}$, which was just formed, represents a square component sub-matrix of the overall state matrix $\underline{\underline{A^{(\ell)}}}$. All component, sub-matrices

$$\underline{\underline{A}}_{\alpha,\beta}^{(\ell)}, (\alpha, \beta) = (1, 4)$$

of the overall state matrix $\underline{\underline{A^{(\ell)}}}$ are defined in the same way as was $\underline{\underline{A}}_{1,3}^{(\ell)}$. (Since the component submatrices can be defined by inspection of (2)–(5), it is not necessary to list the

$$\underline{\underline{A}}_{\alpha,\beta}^{(\ell)}, (\alpha, \beta) = (1, 4)$$

matrices specifically). The overall SV equations, determined from (2)–(5) in the ℓth thin-shell layer, is given by

$$\frac{\partial \underline{\underline{V^{(\ell)}}}}{\partial s_\ell} = \underline{\underline{A^{(\ell)}}}\,\underline{\underline{V^{(\ell)}}}, \qquad \ell = 1, 2, 3, \cdots, L \quad (6)$$

where

$$\underline{\underline{A^{(\ell)}}} = \begin{bmatrix} 0 & 0 & \underline{\underline{A_{1,3}^{(\ell)}}} & \underline{\underline{A_{1,4}^{(\ell)}}} \\ 0 & 0 & \underline{\underline{A_{2,3}^{(\ell)}}} & \underline{\underline{A_{2,4}^{(\ell)}}} \\ \underline{\underline{A_{3,1}^{(\ell)}}} & \underline{\underline{A_{3,2}^{(\ell)}}} & 0 & 0 \\ \underline{\underline{A_{4,1}^{(\ell)}}} & \underline{\underline{A_{4,2}^{(\ell)}}} & 0 & 0 \end{bmatrix}$$

$$\underline{V^{(\ell)}} = \begin{bmatrix} \underline{S_\theta^{(\ell)}} \\ \underline{S_\varphi^{(\ell)}} \\ \underline{U_\theta^{(\ell)}} \\ \underline{U_\varphi^{(\ell)}} \end{bmatrix}. \quad (7)$$

If the overall SV equation is truncated with $|i| \le I_T$ and $|m| \le M_T$, then $\underline{\underline{A^{(\ell)}}}$ is a $P_T \times P_T$ square matrix with

$P_T = 4(2I_T + 1)(2M_T + 1)$. The solution of the overall SV matrix solution is given by

$$\underline{V^{(\ell)}(s_\ell)}_p = \underline{V^{(\ell)}}_p \exp[q_p^{(\ell)} s_\ell]$$

where $q_p^{(\ell)}$ and $\underline{V^{(\ell)}}_p$ $(p = 1, \cdots, P_T)$ are the eigenvalues and eigenvectors, respectively, of the SV matrix $\underline{\underline{A^{(\ell)}}}$. The overall EM-field solution in each thin-shell region can be found by adding a linear combination of the P_T eigensolutions. For example, if $|i| \le I_T$, $|m| \le M_T$, $(p = 1, \cdots, P_T)$, then the $S_\theta^{(2,\ell)}(s_\ell, v, \varphi)$ field is given by $S_\theta^{(2,\ell)}(s_\ell, v, \varphi) = \sum_{i,m,p} C_p^{(\ell)} S_{\theta\,\mathrm{imp}}^{(\ell)} \exp[q_p^{(\ell)} s_\ell + j(i\pi v + m\kappa\varphi)]$ where $S_{\theta\,\mathrm{imp}}^{(\ell)}$ is the pth eigenvector component of $\underline{S_\theta^{(\ell)}}_p$, in the overall eigenvector, $\underline{V^{(\ell)}}_p$ and $C_p^{(\ell)}$ are unknown EM-field expansion coefficients.

Although a large matrix equation could be formed from matching EM boundary conditions at $r = a$, $r = b$, and at each thin-shell layer interface in the inhomogeneous region, a more efficient solution method is to use a ladder approach [18] (i.e., successively relate unknown coefficients from one layer to the next) to express the $C_p^{(L)}$ coefficients of the Lth thin-shell layer (located in the layer adjacent to $r = a$) in terms of the $C_p^{(1)}$ coefficients (located in the layer adjacent to $r = b$), and then match boundary conditions at $r = a$ and $r = b$ interfaces to obtain the final unknowns of the system. At the ℓth and $(\ell + 1)$th interface, matching the tangential magnetic and electric fields, one has

$$\sum_{p=1}^{P_T} C_p^{(\ell)} S_{\theta\mathrm{imp}}^{(\ell)} e^{-q_p^{(\ell)} d_\ell} = \sum_{p=1}^{P_T} C_p^{(\ell+1)} S_{\theta\mathrm{imp}}^{(\ell+1)} \tag{8}$$

$$\sum_{p=1}^{P_T} C_p^{(\ell)} S_{\varphi\mathrm{imp}}^{(\ell)} e^{-q_p^{(\ell)} d_\ell} = \sum_{p=1}^{P_T} C_p^{(\ell+1)} S_{\varphi\mathrm{imp}}^{(\ell+1)} \tag{9}$$

$$\sum_{p=1}^{P_T} C_p^{(\ell)} U_{\theta\mathrm{imp}}^{(\ell)} e^{-q_p^{(\ell)} d_\ell} = \sum_{p=1}^{P_T} C_p^{(\ell+1)} U_{\theta\mathrm{imp}}^{(\ell+1)} \tag{10}$$

$$\sum_{p=1}^{P_T} C_p^{(\ell)} U_{\varphi\mathrm{imp}}^{(\ell)} e^{-q_p^{(\ell)} d_\ell} = \sum_{p=1}^{P_T} C_p^{(\ell+1)} U_{\varphi\mathrm{imp}}^{(\ell+1)}. \tag{11}$$

Letting $\underline{C^{(\ell)}} = [C_1^{(\ell)}, \cdots, C_{P_T}^{(\ell)}]^t$, these equations may be written

$$\underline{\underline{D_-^{(\ell)}}}\ \underline{C^{(\ell)}} = \underline{\underline{D_+^{(\ell)}}}\ \underline{C^{(\ell+1)}} \tag{12}$$

or

$$\begin{aligned}\underline{C^{(\ell+1)}} &= \left[\underline{\underline{D_+^{(\ell)}}}\right]^{-1} \underline{\underline{D_-^{(\ell)}}}\ \underline{C^{(\ell)}} \\ &= \underline{\underline{F^{(\ell)}}}\ \underline{C^{(\ell)}}, \qquad \ell = 1, \cdots, L-1\end{aligned} \tag{13}$$

where the -1 superscript denotes matrix inverse. Substituting successively, one has

$$\begin{aligned}\underline{C^{(L)}} &= \underline{\underline{F^{(L-1)} F^{(L-2)}}}\{, \cdots, [\underline{\underline{F^{(1)}}}\ \underline{C^{(1)}}], \cdots, \} \\ &= \underline{\underline{M}}\ \underline{C^{(1)}}.\end{aligned} \tag{14}$$

Another important problem is to relate the fields of Region 1 (interior region) and Region 3 (exterior region) to the fields of Region 2 (inhomogeneous region). The fields in Regions 1 and 3, as is well known, can be expressed in terms of an infinite number of *transverse to r electric* (TE_r) and *transverse to r magnetic* (TM_r) Schelkunoff spherical-vector potential modes [3, Ch. 6]. These vector potential modes consist of half-order radial Bessel and Hankel functions and consist of Tesseral harmonics (products of Legendre polynomials and φ exponential functions). The scattered field portions of the Region–1 and Region–3 Bessel- and Hankel-function solution are chosen to satisfy the usual spherical boundary conditions of finiteness at the origin, and being an outgoing wave at infinity. In this paper, the incident field in Region 1 is the EM field of an infinitesimal dipole. The basic EM boundary-matching procedure to be followed in this paper is to equate the tangential electric fields at the interfaces $r = a$ and $r = b$, eliminate unknown field constants in Regions 1 and 3 in favor of the field constants in Region 2 from these equations, equate the tangential magnetic fields at the interfaces $r = a$ and $r = b$, substitute the electric-field matching Region 2 constants into the magnetic-field matching equations. This general procedure is precisely the one followed by [15], [18], [20] in the analysis of diffraction from planar diffraction gratings. Equating the common terms of $\exp(j\kappa m\varphi)$ of the $S_{\theta m}(v)$ and $S_{\varphi m}(v)$ field components at $r = a$ from Regions 1 and 2, one has

$$\begin{aligned}S_{\theta m}^{(1)}(v) &= S_{\theta m}^{(1,\mathrm{Scat})}(v) + S_{\theta m}^{(1,\mathrm{INC})}(v) \\ &= S_{\theta m}^{(2,a)}(v)\end{aligned} \tag{15}$$

$$\begin{aligned}S_{\varphi m}^{(1)}(v) &= S_{\varphi m}^{(1,\mathrm{Scat})}(v) + S_{\varphi m}^{(1,\mathrm{INC})}(v) \\ &= S_{\varphi m}^{(2,a)}(v)\end{aligned} \tag{16}$$

where

$$\begin{aligned}&S_{\theta m}^{(1,\mathrm{Scat})}(v) \\ &\quad = \sum_{i=-I_T}^{I_T} \left\{ \sum_{n=|\kappa m|+\delta_{m,0}}^{2I_T+|\kappa m|+\delta_{m,0}} [E_{Aimn}^{(1)} F_{mn}^{(1)} + E_{Bimn}^{(1)} A_{mn}^{(1)}] \right\} \\ &\qquad \cdot \exp(ji\pi v)\end{aligned} \tag{17}$$

$$\begin{aligned}&S_{\varphi m}^{(1,\mathrm{Scat})}(v) \\ &\quad = \sum_{i=-I_T}^{I_T} \left\{ \sum_{n=|\kappa m|+\delta_{m,0}}^{2I_T+|\kappa m|+\delta_{m,0}} \left[E_{Cimn}^{(1)} F_{mn}^{(1)} + E_{Dimn}^{(1)} A_{mn}^{(1)}\right] \right\} \\ &\qquad \cdot \exp(ji\pi v)\end{aligned} \tag{18}$$

where

$$E_{\mathrm{Aim}}^{(1)} = \frac{-jm}{\varepsilon_1} \hat{J}_n(\beta_1 a) g_{imn}^A$$

$$E_{Bim}^{(1)} = \frac{-j}{\beta_1} \hat{J}_n'(\beta_1 a) g_{imn}^B$$

$$E_{Cim}^{(1)} = \frac{1}{\varepsilon_1} \hat{J}_n(\beta_1 a) g_{imn}^C$$

and

$$E_{\mathrm{Dim}}^{(1)} = \frac{\kappa m}{\beta_1} \hat{J}_n'(\beta_1 a) g_{imn}^D.$$

Letting $g_{Amn} = (1 - v^2)^{-1/2} P_n^{|\kappa m|}(v)$, $g_{Bmn} = -(1 - v^2)^{1/2} \partial/\partial v[P_n^{|\kappa m|}(v)]$, $g_{Cmn} = -(1 - v^2) \partial/\partial v[P_n^{|\kappa m|}(v)]$,

and $g_{Dmn} = P_n^{|\kappa m|}(v)$ where $P_n^{|\kappa m|}(v)$ are associated Legendre functions [3] of order n and $|\kappa m|$, the coefficients g_{imn}^A, g_{imn}^B, g_{imn}^C, and g_{imn}^D represent the exponential Fourier series-expansion coefficients for the terms $g_{Amn}(v)$, $g_{Bmn}(v)$, $g_{Cmn}(v)$, and $g_{Dmn}(v)$, respectively, on the interval $-1 \leq v \leq 1$ [$g_{Amn}(v) = \sum_i g_{imn}^A \exp(ji\pi v)$]. In the present analysis, the Fourier coefficients g_{imn}^A, g_{imn}^B, g_{imn}^C, and g_{imn}^D have been determined *exactly* by calculating higher order derivatives of the Bessel-function integral representation given in [22, eq. (9.1.20), p. 360]. The exact calculation of these Fourier coefficients is an important step in order to ensure overall accuracy of the entire RCWT algorithm. The terms

$$S_{\theta m}^{(1,\mathrm{INC})}(v) = \sum_i S_{\theta im}^{(1,\mathrm{INC})} \exp(ji\pi v)$$

and

$$S_{\varphi m}^{(1,\mathrm{INC})}(v) = \sum_i S_{\varphi im}^{(1,\mathrm{INC})} \exp(ji\pi v)$$

represent electric-field EM incident waves evaluated at $r = a$, which emanate from Region 1. In this paper, it is assumed that a centered electric dipole excites EM radiation in the overall system and for this source it is found $S_{\theta m}^{(1,\mathrm{INC})}(v) = (j/\beta_1)A_{0,1}^I \hat{H}_1'(\beta_1 a)[1-v^2]^{1/2}\delta_{m,0}$, $S_{\varphi m}^{(1,\mathrm{INC})}(v) = 0$, and $A_{0,1}^I$ is the strength of the electric-dipole source. In (15)–(18), $\beta_1 = \sqrt{\mu_1 \varepsilon_1}$, $\hat{J}_n(\beta_1 a)$ are spherical Schelkunoff–Bessel functions [3], the prime in (15)–(18) represents differentiation with regard to the argument. For $m \neq 0$, the lower n limits start at $|\kappa m|$ since the Legendre polynomials are zero when $|\kappa m| > n$. The terms $S_{\theta m}^{(2,a)}(v)$ and $S_{\varphi m}^{(2,a)}(v)$ represent the SV solution in Region 2 in the Lth thin-shell layer region evaluated at $r = a$ and are given by

$$\begin{aligned} S_{\theta m}^{(2,a)}(v) &= \sum_{i=-I_T}^{I_T} \left\{ \sum_{p=1}^{P_T} C_p^{(L)} S_{\theta\mathrm{imp}}^{(L)} \exp[-q_p^{(L)} s_L] \right\} \cdot \exp(ji\pi v) \\ &= \sum_{i=-I_T}^{I_T} S_{\theta im}^{(2,a)} \exp(ji\pi v) \end{aligned} \tag{19}$$

$$\begin{aligned} S_{\varphi m}^{(2,a)}(v) &= \sum_{i=-I_T}^{I_T} \left\{ \sum_{p=1}^{P_T} C_p^{(L)} S_{\varphi\mathrm{imp}}^{(L)} \exp[-q_p^{(L)} s_L] \right\} \cdot \exp(ji\pi v) \\ &= \sum_{i=-I_T}^{I_T} S_{\varphi im}^{(2,a)} \exp(ji\pi v). \end{aligned} \tag{20}$$

When I_T is infinite, the boundary matching equations given by (15)–(20) are exact. When I_T is truncated at a finite value, and common coefficients of $\exp(ji\pi v)$ in (15)–(20) are collected, (15)–(20) give a $[2(2I_T+1)] \times [2(2I_T+1)]$ set of equations from which the $A_{mn}^{(1)}$ and $F_{mn}^{(1)}$ can be expressed in terms of the Region–2 unknown coefficients $C_p^{(L)}$. Letting $\underline{\underline{E_{Am}^{(1)}}}$, $\underline{\underline{E_{Bm}^{(1)}}}$, $\underline{\underline{E_{Cm}^{(1)}}}$, and $\underline{\underline{E_{Dm}^{(1)}}}$ be matrices representing (17), (18), e.g., $\underline{\underline{E_{Am}^{(1)}}} = [E_{Aimn}^{(1)}]$, where $i = -I_T, \cdots, I_T$ and $n = |\kappa m| + \delta_{m,0}, \cdots, 2I_T + |\kappa m| + \delta_{m,0}\}$, letting $\underline{S_{\theta m}^{(1,\mathrm{INC})}} = [S_{\theta im}^{(1,\mathrm{INC})}]$ and $\underline{S_{\varphi m}^{(1,\mathrm{INC})}} = [S_{\varphi im}^{(1,\mathrm{INC})}]$ for $i = -I_T, \cdots, I_T$, and letting $\underline{\underline{S_{\theta m}^{(2,a)}}} = \{S_{\theta\mathrm{imp}}^{(L)} \exp[-q_p^{(L)} s_L]\}$, $\underline{\underline{S_{\varphi m}^{(2,a)}}} = \{S_{\varphi\mathrm{imp}}^{(L)} \exp[-q_p^{(L)} s_L]\}$ for $i = -I_T, \cdots, I_T$ and $p = 1, \cdots, P_T$, one finds the following matrix equation:

$$\begin{aligned} \underline{\underline{S_m^{(2,a)}}}\,\underline{C^{(L)}} &= \begin{bmatrix} \underline{\underline{S_{\theta m}^{(2,a)}}} \\ \underline{\underline{S_{\varphi m}^{(2,a)}}} \end{bmatrix} \underline{C^{(L)}} \\ &= \begin{bmatrix} \underline{\underline{E_{Am}^{(1)}}} & \underline{\underline{E_{Bm}^{(1)}}} \\ \underline{\underline{E_{Cm}^{(1)}}} & \underline{\underline{E_{Dm}^{(1)}}} \end{bmatrix} \begin{bmatrix} \underline{F_m^{(1)}} \\ \underline{A_m^{(1)}} \end{bmatrix} + \begin{bmatrix} \underline{S_\theta^{(1,\mathrm{INC})}} \\ \underline{S_\varphi^{(1,\mathrm{INC})}} \end{bmatrix} \\ &= \underline{\underline{E_m^{(1)}}} \begin{bmatrix} \underline{F_m^{(1)}} \\ \underline{A_m^{(1)}} \end{bmatrix} + \underline{S_m^{(1,\mathrm{INC})}} \end{aligned} \tag{21}$$

where $\underline{\underline{S_m^{(2,a)}}}$ is a $[2(2I_T+1)] \times P_T$ matrix, $\underline{\underline{E_m^{(1)}}}$ is a $[2(2I_T+1)] \times [2(2I_T+1)]$ square matrix, and $\underline{S_m^{(1,\mathrm{INC})}}$ is a $2(2I_T+1)$ column matrix.

To proceed further, one matches the terms common to $\exp(j\kappa m\varphi)$ of the tangential magnetic field at the Region-1, Region-2 interface at $r = a$ and finds

$$\begin{aligned} U_{\theta m}^{(1)}(v) &= U_{\theta m}^{(1,\mathrm{Scat})}(v) + U_{\theta m}^{(1,\mathrm{INC})}(v) \\ &= U_{\theta m}^{(2,a)}(v) \end{aligned} \tag{22}$$

$$\begin{aligned} U_{\varphi m}^{(1)}(v) &= U_{\varphi m}^{(1,\mathrm{Scat})}(v) + U_{\varphi m}^{(1,\mathrm{INC})}(v) \\ &= U_{\varphi m}^{(2,a)}(v) \end{aligned} \tag{23}$$

where

$$\begin{aligned} &U_{\theta m}^{(1,\mathrm{Scat})}(v) \\ &\quad = \sum_{i=-I_T}^{I_T} \left\{ \sum_{n=|\kappa m|+\delta_{m,0}}^{2I_T+|\kappa m|+\delta_{m,0}} [H_{Bimn}^{(1)} F_{mn}^{(1)} + H_{Aimn}^{(1)} A_{mn}^{(1)}] \right\} \\ &\qquad \cdot \exp(ji\pi v) \end{aligned} \tag{24}$$

$$\begin{aligned} &U_{\varphi m}^{(1,\mathrm{Scat})}(v) \\ &\quad = \sum_{i=-I_T}^{I_T} \left\{ \sum_{n=|\kappa m|+\delta_{m,0}}^{2I_T+|\kappa m|+\delta_{m,0}} \left[H_{Dimn}^{(1)} F_{mn}^{(1)} + H_{Cimn}^{(1)} A_{mn}^{(1)}\right] \right\} \\ &\qquad \cdot \exp(ji\pi v) \end{aligned} \tag{25}$$

where

$$\begin{aligned} H_{\mathrm{Aim}}^{(1)} &= \frac{j\kappa m}{\mu_1} \hat{J}_n(\beta_1 a) g_{imn}^A \\ H_{Bim}^{(1)} &= \frac{-j}{\beta_1} \hat{J}_n'(\beta_1 a) g_{imn}^B \\ H_{Cim}^{(1)} &= \frac{-1}{\mu_1} \hat{J}_n(\beta_1 a) g_{imn}^C \end{aligned}$$

and

$$H_{\mathrm{Dim}}^{(1)} = \frac{\kappa m}{\beta_1} \hat{J}_n'(\beta_1 a) g_{imn}^D.$$

The terms $U_{\theta m}^{(1,\mathrm{INC})}(v) = \sum_i U_{\theta im}^{(1,\mathrm{INC})} \exp(ji\pi v)$ and $U_{\varphi m}^{(1,\mathrm{INC})}(v) = \sum_i U_{\varphi im}^{(1,\mathrm{INC})} \exp(ji\pi v)$ represent the magnetic-field incident waves which may emanate from Region 1. In this paper, $U_{\varphi m}^{(1,\mathrm{INC})}(v) = (1/\mu_1) A_{0,1}^I \hat{H}_1(\beta_1 a)[1-v^2]\delta_{m,0}$ and $U_{\theta m}^{(1,\mathrm{INC})}(v) = 0$ for a centered electric-dipole source. The terms $U_{\theta m}^{(2,a)}(v)$ and

$U_{\varphi m}^{(2,a)}(v)$ represent the SV solution in Region 2 in the Lth thin-shell layer region evaluated at $r=a$ and are given by

$$U_{\theta m}^{(2,a)}(v) = \sum_{i=-I_T}^{I_T} \left\{ \sum_{p=1}^{P_T} C_p^{(L)} U_{\theta \text{imp}}^{(L)} \exp\left[-q_p^{(L)} s_L\right] \right\} \cdot \exp(ji\pi v) = \sum_{i=-I_T}^{I_T} U_{\theta im}^{(2,a)} \exp(ji\pi v) \tag{26}$$

$$U_{\varphi m}^{(2,a)}(v) = \sum_{i=-I_T}^{I_T} \left\{ \sum_{p=1}^{P_T} C_p^{(L)} U_{\varphi \text{imp}}^{(L)} \exp\left[-q_p^{(L)} s_L\right] \right\} \cdot \exp(ji\pi v) = \sum_{i=-I_T}^{I_T} U_{\varphi im}^{(2,a)} \exp(ji\pi v). \tag{27}$$

Equating common coefficients of $\exp(ji\pi v)$ in (22)–(27), a similar matrix equation as was formed for the tangential electric-field components may be formed for the tangential magnetic-field components. One has

$$\underline{\underline{U_m^{(2,a)}}}\ \underline{C^{(L)}} = \begin{bmatrix} \underline{\underline{U_{\theta m}^{(2,a)}}} \\ \underline{\underline{U_{\varphi m}^{(2,a)}}} \end{bmatrix} \underline{C^{(L)}} = \begin{bmatrix} \underline{\underline{H_{Bm}^{(1)}}} & \underline{\underline{H_{Am}^{(1)}}} \\ \underline{\underline{H_{Dm}^{(1)}}} & \underline{\underline{H_{Cm}^{(1)}}} \end{bmatrix} \begin{bmatrix} \underline{F_m^{(1)}} \\ \underline{A_m^{(1)}} \end{bmatrix} + \begin{bmatrix} \underline{U_\theta^{(1,\text{INC})}} \\ \underline{U_\varphi^{(1,\text{INC})}} \end{bmatrix} = \underline{\underline{H_m^{(1)}}} \begin{bmatrix} \underline{F_m^{(1)}} \\ \underline{A_m^{(1)}} \end{bmatrix} + \underline{U_m^{(1,\text{INC})}}. \tag{28}$$

To proceed further, this paper's objective now is to eliminate the column matrix $[\underline{F_m^{(1)}}, \underline{A_m^{(1)}}]^t$ from (21) and, therefore, form a single matrix equation for the $\underline{C^{(L)}}$ coefficients alone. By inspecting the matrix equation (21) and their definitions, one notices that two distinct cases arise, namely the cases when $m \neq 0$ and the case when $m = 0$. In the case of $m \neq 0$, it turns out that the matrices $\underline{\underline{E_m^{(1)}}}$ and $\underline{\underline{H_m^{(1)}}}$ are nonsingular, therefore, it is straightforward to invert $\underline{\underline{E_m^{(1)}}}$ and solve for $[\underline{F_m^{(1)}}, \underline{A_m^{(1)}}]^t$. For $m \neq 0$, one finds

$$\begin{bmatrix} \underline{F_m^{(1)}} \\ \underline{A_m^{(1)}} \end{bmatrix} = \underline{\underline{E_m^{(1)}}}^{-1} [\underline{\underline{S^{(2,a)}}}\ \underline{C^{(L)}}] - \underline{\underline{E_m^{(1)}}}^{-1} \underline{S_m^{(1,\text{INC})}} = \underline{\underline{Z_m^{(1)}}}\ \underline{C^{(L)}} - \underline{E_m^{(1,\text{INC})}}. \tag{29}$$

The determination of $F_{0,n}^{(1)}$ and $A_{0,n}^{(1)}$ $(n = 1, 2, 3, \cdots)$ coefficients for the $m = 0$ case requires special matrix processing. One first notes for the $m = 0$ case that $E_{\text{Aim}}^{(1)} = E_{\text{Dim}}^{(1)} = 0$ in (17), (18), and thus, the matrix equations for $F_{0,n}^{(1)}$ and $A_{0,n}^{(1)}$ are decoupled from one another. One also observes from (17), (18) that when solving for either $F_{0,n}^{(1)}$ and $A_{0,n}^{(1)}$, that the coefficients of $F_{0,1}^{(1)}, F_{0,3}^{(1)}, F_{0,5}^{(1)}, \cdots$, and $A_{0,1}^{(1)}, A_{0,3}^{(1)}, A_{0,5}^{(1)}, \cdots$, are multiplied by the first derivative Legendre polynomials $\partial/\partial v\ [P_1^0(v)]$, $\partial/\partial v\ [P_3^0(v)], \cdots$, which are even in v, whereas the coefficients of $F_{0,2}^{(1)}, F_{0,4}^{(1)}, F_{0,6}^{(1)}, \cdots$, and $A_{0,2}^{(1)}, A_{0,4}^{(1)}, A_{0,6}^{(1)}, \cdots$, are multiplied by first derivative in Legendre polynomials $\partial/\partial v\ [P_2^0(v)]$, $\partial/\partial v[P_4^0(v)], \cdots$, which are odd in v. This means that when determining the $m = 0$, Region-1 coefficients $F_{0,n}^{(1)}$ and $A_{0,n}^{(1)}$, that the best numerical processing in (21) is to decompose $S_{\theta m}^{(1,\text{INC})}(v)$, $S_{\varphi m}^{(1,\text{INC})}(v)$, $S_{\theta m}^{(2,a)}(v)$, $S_{\varphi m}^{(2,a)}(v)$ for $m = 0$ into a sum of even and odd functions, and from the even functions in (17), (18) determine $F_{0,1}^{(1)}, F_{0,3}^{(1)}, F_{0,5}^{(1)}, \cdots$, and $A_{0,1}^{(1)}, A_{0,3}^{(1)}, A_{0,5}^{(1)}, \cdots$, and from the odd functions in (17), (18) determine $F_{0,2}^{(1)}, F_{0,4}^{(1)}, F_{0,6}^{(1)}, \cdots$, and $A_{0,2}^{(1)}, A_{0,4}^{(1)}, A_{0,6}^{(1)}, \cdots$. The specific matrix processing that is carried out for, say, the $F_{0,1}^{(1)}, F_{0,3}^{(1)}, F_{0,5}^{(1)}, \cdots$, coefficients is as follows. After decomposing $S_{\varphi m}^{(1,\text{INC})}(v)$ and $S_{\varphi m}^{(2,a)}(v)$ for $m = 0$ into even and odd functions of v, $F_{0,1}^{(1)}, F_{0,3}^{(1)}, F_{0,5}^{(1)}, \cdots$, is determined by: 1) expanding the even function part of $S_{\varphi m}^{(1,\text{INC})}(v)$ and $S_{\varphi m}^{(2,a)}(v)$ for $m = 0$ in a $\{\cos(i\pi v)\}_{i=0}^{I_T}$ cosine series (The $\{\cos(i\pi v)\}_{i=0}^{I_T}$ series expansion of $S_{\varphi m}^{(2,a)}(v)$ for $m = 0$ depends on the $C_p^{(L)}$, $p = 1, \cdots, P_T$ coefficients in Region 2 and the $\{\cos(i\pi v)\}_{i=0}^{I_T}$ series expansion of $S_{\varphi m}^{(1,\text{INC})}(v)$ for $m = 0$ depends on the incident EM-source waves which emanate from Region 1.); 2) expanding the first derivative Legendre polynomial $\partial/\partial v[P_1^0(v)]$, $\partial/\partial v[P_3^0(v)], \cdots$, in a $\{\cos(i\pi v)\}_{i=0}^{I_T}$ series; 3) equating common coefficients of the cosine series $\{\cos(i\pi v)\}_{i=0}^{I_T}$; and 4) from these equations, developing an $(I_T+1)x(I_T+1)$ matrix equation, which upon matrix inversion expresses the $F_{0,1}^{(1)}, F_{0,3}^{(1)}, F_{0,5}^{(1)}, \cdots$, coefficients in terms of the $C_p^{(L)}$, $p = 1, \cdots, P_T$ coefficients of Region 2 and incident EM-wave coefficients of Region 1. The determination of the $F_{0,2}^{(1)}, F_{0,4}^{(1)}, F_{0,6}^{(1)}, \cdots$, coefficients is found by: 1) expanding the odd-function part of $S_{\varphi m}^{(1,\text{INC})}(v)$ and $S_{\varphi m}^{(2,a)}(v)$ for $m = 0$ and the odd derivative Legendre polynomials $\partial/\partial v[P_2^0(v)]$, $\partial/\partial v[P_4^0(v)]$ functions in a $\{\sin(i\pi v)\}_{i=1}^{I_T}$ series; 2) equating common coefficients of $\{\sin(i\pi v)\}_{i=1}^{I_T}$; and 3) and then forming an $I_T \times I_T$ matrix equation which, upon matrix inversion, expresses the $F_{0,2}^{(1)}, F_{0,4}^{(1)}, F_{0,6}^{(1)}, \cdots$, coefficients in terms of the $C_p^{(L)}$, $p = 1, \cdots, P_T$ coefficients of Region 2 and incident EM-wave coefficients of Region 1. After following the above procedure, and combining the even- and odd-matrix expressions for $F_{0,1}^{(1)}, F_{0,3}^{(1)}, F_{0,5}^{(1)}, \cdots$, and $F_{0,2}^{(1)}, F_{0,4}^{(1)}, F_{0,6}^{(1)}, \cdots$, a $(2I_T+1)\times(2I_T+1)$ matrix relation is found between the overall $F_{0,1}^{(1)}, F_{0,2}^{(1)}, F_{0,3}^{(1)}, F_{0,4}^{(1)}, \cdots$, coefficients and the $C_p^{(L)}$, $p = 1, \cdots, P_T$ coefficients and EM-incident-wave coefficients of Region 1. A similar even and odd analysis allows a $(2I_T+1)\times(2I_T+1)$ matrix relation between the $A_{0,n}^{(1)}$ coefficients and the $C_p^{(L)}$, $p = 1, \cdots, P_T$ coefficients of Region 2 and EM-incident-wave coefficients of Region 1. Altogether the $F_{0,n}^{(1)}$ and $A_{0,n}^{(1)}$ coefficients for $m = 0$ in matrix form may be expressed as

$$\begin{bmatrix} \underline{F_0^{(1)}} \\ \underline{A_0^{(1)}} \end{bmatrix} = \begin{bmatrix} \underline{\underline{Z_0^{(1,F)}}} & 0 \\ 0 & \underline{\underline{Z_0^{(1,A)}}} \end{bmatrix} \underline{C^{(L)}} - \underline{E_0^{(1,\text{INC})}} = \underline{\underline{Z_0^{(1)}}}\ \underline{C^{(L)}} - \underline{E_0^{(1,\text{INC})}} \tag{30}$$

where the matrix $\underline{\underline{Z_0^{(1)}}}$ is size $[2(2I_T+1)]\times[2(2I_T+1)]$. Substituting $[\underline{F_m^{(1)}}\ \ \underline{A_m^{(1)}}]^t$ from (29) ($m\neq 0$) and $[\underline{F_0^{(1)}}\ \ \underline{A_0^{(1)}}]^t$ of (30) ($m=0$) into (28) one finds

$$[\underline{\underline{U_m^{(2,a)}}}-\underline{\underline{H_m^{(1)}Z_m^{(1)}}}]\underline{C^{(L)}}=\underline{U_m^{(1,\mathrm{INC})}}-\underline{\underline{H_m^{(1)}}}\,\underline{E_m^{(1,\mathrm{INC})}} \quad (31)$$

where $m=-M_T,\cdots,-1,0,1,\cdots,M_T$. For each m, (31) has $2(2I_T+1)$ rows.

The boundary matching analysis at the $r=b$ interface is identical to that at $r=a$ and the boundary matching equations at the $r=b$ interface are given by (15)–(31) if: 1) one replaces *Region-1* superscripts with *Region-3* superscripts; 2) one replaces the spherical Schelkunoff–Bessel function $\hat{J}_n(\beta_1 a)$ with the outgoing spherical Schelkunoff–Hankel function of the second kind, namely $\hat{H}_n(\beta_3 b)$; 3) one replaces $S_{\theta m}^{(2,a)}(v)$ and $S_{\varphi m}^{(2,a)}(v)$ in (19), (20) with the $\ell=1$ thin-shell SV solution evaluated at $r=b$, namely

$$\begin{aligned}S_{\theta m}^{(2,b)}(v)&=\sum_{i=-I_T}^{I_T}\left\{\sum_{p=1}^{P_T}C_p^{(1)}S_{\theta\mathrm{imp}}^{(1)}\right\}\exp(ji\pi v)\\&=\sum_{i=-I_T}^{I_T}S_{\theta im}^{(2,b)}\exp(ji\pi v)\end{aligned}\quad(32)$$

$$\begin{aligned}S_{\varphi m}^{(2,b)}(v)&=\sum_{i=-I_T}^{I_T}\left\{\sum_{p=1}^{P_T}C_p^{(1)}S_{\varphi\mathrm{imp}}^{(1)}\right\}\exp(ji\pi v)\\&=\sum_{i=-I_T}^{I_T}S_{\varphi im}^{(2,b)}\exp(ji\pi v)\end{aligned}\quad(33)$$

and 4) one sets all Region-3 incident source terms to zero since EM energy in this paper is assumed to emanate only from a Region-1 centered-dipole source. After algebra, it is found that the Region-3 boundary equations are

$$[\underline{\underline{U_m^{(2,b)}}}-\underline{\underline{H_m^{(3)}Z_m^{(3)}}}]\underline{C^{(1)}}=\underline{U_m^{(3,\mathrm{INC})}}-\underline{\underline{H_m^{(3)}}}\,\underline{E_m^{(3,\mathrm{INC})}} \quad (34)$$

where $m=-M_T,\cdots,-1,0,1,\cdots,M_T$ and where the RHS of (34) for this paper is zero. For each m, (34) has $2(2I_T+1)$ rows. Using $\underline{C^{(L)}}=\underline{\underline{M}}\,\underline{C^{(1)}}$ from (14), one eliminates the $\underline{C^{(L)}}$ column matrix and find

$$[\underline{\underline{U_m^{(2,a)}}}-\underline{\underline{H_m^{(1)}Z_m^{(1)}}}]\underline{\underline{M}}\,\underline{C^{(1)}}=\underline{U_m^{(1,\mathrm{INC})}}-\underline{\underline{H_m^{(1)}}}\,\underline{E_m^{(1,\mathrm{INC})}} \quad (35)$$

where $m=-M_T,\cdots,-1,0,1,\cdots,M_T$. Including all values of m, (34) and (35) each represent $[2M_T+1]\times[2(2I_T+1)]=P_T/2$ equations for $\underline{C^{(1)}}$. Thus, (34) and (35) represent together, a $P_T\times P_T$ matrix equation from which $\underline{C^{(1)}}$ may be determined. From knowledge of $\underline{C^{(1)}}$ all other unknown constants of the system may be determined.

Once all of the EM-field coefficients are determined, one may calculate the power which is radiated in Regions 1 and 3 of the system. The radiated power, which is associated with a given m and n spherical mode, is well known and the specific formulas may be found in [3, Ch. 6]. In this paper, numerical results will be given in terms of normalized power. The normalized power of a given m and n spherical mode at radial distance r is defined here as the power which is radiated by the m and n spherical mode into a sphere located at a radius r *divided* by the total power radiated by the centered dipole when the centered dipole is in an infinite region whose material parameters are those of Region 1, namely ε_1 and μ_1.

III. Numerical Results

In this section, the RCWT method of Section II is illustrated by solving for the radiated and scattered EM fields, that result when the Region-2 inhomogeneous-material shell is assumed to have, as a specific example, the form

$$\begin{aligned}\varepsilon(r,\theta,\varphi)&=\varepsilon_2+\Delta\varepsilon_\theta\sin(\theta)\,\mathrm{sgn}[\cos(\theta)]\\&\quad\cdot[1+\Delta\varepsilon_\varphi(r)\,\mathrm{sgn}(\varphi)]\\&=\varepsilon_2+\Delta\varepsilon_\theta[1-v^2]^{1/2}\,\mathrm{sgn}(v)\\&\quad\cdot[1+\Delta\varepsilon_\varphi(r)\,\mathrm{sgn}(\varphi)],\\\mu(r,\theta,\varphi)&=\mu_2\end{aligned}\quad(36)$$

where $\mathrm{sgn}(X)=1$, $X>0$ and $\mathrm{sgn}(X)=-1$, $X<0$. For this profile, $\kappa=1$. This inhomogeneity profile is a convenient one to use, since if it is integrated over a spherical surface of radius r, its average or bulk value is always ε_2, regardless of the value of $\Delta\varepsilon_\theta$ or $\Delta\varepsilon_\varphi$ used. Using this dielectric inhomogeneity profile, three cases will be studied—namely the cases when: $\Delta\varepsilon_\theta=0.001$, $\Delta\varepsilon_\varphi(r)=0.001$ (Case 1); $\Delta\varepsilon_\theta=2.8$, $\Delta\varepsilon_\varphi(r)=0.4$ (Case 2); and $\Delta\varepsilon_\theta=2.8$, $\Delta\varepsilon_\varphi(r)=\alpha_1 r+\alpha_2$ (Case 3), where $\Delta\varepsilon_\varphi(r)|_{r=5}=0.6$ and $\Delta\varepsilon_\varphi(r)|_{r=5.5}=0.15$ for $a\le r\le b$, $a=5$ and $b=5.5$. For all numerical examples of this paper, the bulk material parameters will be taken to be $\varepsilon_1=1.5$, $\mu_1=1$, $\varepsilon_2=7$, $\mu_2=1.3$, $\varepsilon_3=1$, and $\mu_3=1$. The first case, which because of the small values of $\Delta\varepsilon_\theta$ and $\Delta\varepsilon_\varphi$, may be called a homogeneous-profile case, represents the application of the RCWT method to the solution of the problem of determining the EM radiation that occurs when a centered dipole radiates through a uniform dielectric shell. Since this problem of EM radiation through a homogeneous dielectric shell can be solved exactly by matching Bessel-function solutions in Regions 1, 2, and 3, comparison of the RCWT method with the exact Bessel-function matching solution represents a numerical validation of the RCWT method if close numerical results from the two methods occur.

The second case, which may be designated a (θ,φ)-inhomogeneity-profile case, represents an inhomogeneous example in which the dielectric shell is homogeneous in the radial r direction, but is inhomogeneous in the θ and φ coordinates. This case will be solved by both a single-layer RCWT algorithm and will be solved by a using multilayer RCWT algorithm. The purpose of solving this second case is to observe, in general, how much diffraction occurs in higher order spherical modes when a reasonably large θ and φ inhomogeneity-material profile is present in the dielectric shell. The purpose of comparing single-layer and multilayer RCWT results is to observe the importance that the scale factors of (2)–(5) have on the overall scattering solution. The purpose is also to study how well the power conservation law is obeyed numerically. Power conservation at different radial distances is a good indication of the accuracy of the numerical solution in a lossless system such as the present one.

The third case, which may be designated a (r, θ, φ)-inhomogeneity-profile case, represents a solution of the RCWT method under the most general conditions, namely when the inhomogeneity variation occurs in the r, θ, and φ coordinates. The radial inhomogeneity variation has been chosen to vary in such a way that the magnitude of the φ variation in the inhomogeneity-profile changes linearly. Single and multilayer analyses have been studied in order to gauge the effect of the radial inhomogeneity variation of the (r, θ, φ)-inhomogeneity-profile case relative to that of the (θ, φ)-inhomogeneity-profile case. The purpose of studying this case is to see the effect, in general, that a fully 3-D inhomogeneity variation has on diffraction and scattering into higher orders. The purpose also of Case 3, as in Case 2, is to study how well the power conservation law is obeyed numerically.

Fig. 2 shows a comparison of the normalized power radiated through a uniform-material shell when calculated by a Bessel-function matching algorithm (exact solution), when calculated by a single-layer RCWT analysis, and when calculated by a multilayer RCWT analysis. Ten layers ($L = 10$) were used to make all multilayer calculations in this paper. In Fig. 2, the normalized power by all methods has been calculated both at $r = a$ and $r = b$ (The label $r = a, b$ means calculated at $r = a$ and calculated at $r = b$). In Fig. 2, the outer radius is fixed at $b = 5.5$ (radians or rad) and the inner radius a is varied from 5 to 5.45 rad. As can be seen from Fig. 2, one notices that there is excellent numerical agreement between the three methods used. One also notices from Fig. 2 that the $r = a, b$ power results for each of the three methods are so close at $r = a$ and $r = b$ that the two power curves for each method cannot be distinguished from one another. In Fig. 2, the RCWT algorithm was calculated using $M_T = 1$ and $I_T = 5$. Because the inhomogeneity factor in this case was very close to that of a perfectly homogeneous shell, the RCWT algorithm could have calculated the power of this case using a value of $M_T = 0$ and $I_T = 5$, which would have meant a significantly smaller matrix equation than would have resulted from $M_T = 1$. A larger matrix equation than necessary was solved for this case in order to test the numerical stability of the algorithm and also to test the sensitivity of the RCWT solution to error in the Fourier coefficients. (Error in the Fourier coefficients would arise for $M_T = 1$ because numerical integration is used to calculate the $\exp(jm\varphi)$, $m = -1, 0, 1$ Fourier coefficients, and thus, instead of the $m = \pm 1$ coefficients being exactly zero, they would have some small value.) The $M_T = 1$ matrix solution showed no ill-conditioned effects from using a larger than needed matrix size and showed no sensitivity to error in the Fourier coefficients. A RCWT analysis was also carried out using $M_T = 1$ and $I_T = 2$. In this case, the RCWT algorithm differed perceptibly from the Bessel matching solution. This indicates that for accurate results, enough Fourier harmonic terms must be included to correctly calculate the SV solution of (2)–(5).

Fig. 3 shows a comparison of the total normalized powers that occur when the dielectric shell is taken to be a uniform layer (the power here is calculated at $r = b$ by Bessel-function matching) and when the dielectric shell is taken to be a (θ, φ)-inhomogeneity profile with $\Delta\varepsilon_\theta = 2.8$, $\Delta\varepsilon_\varphi(r) = 0.4$

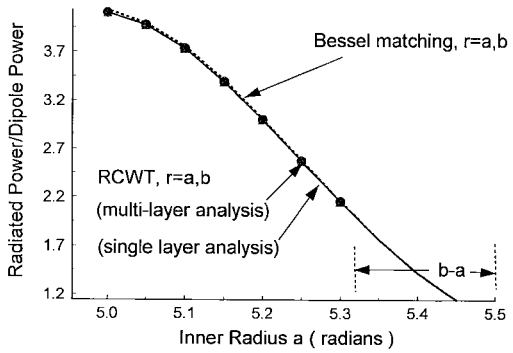

Fig. 2. Normalized total power as obtained by the RCWT method compared to the total normalized power as obtained by matching Bessel-function solutions at the interfaces $r = a$ and $r = b$.

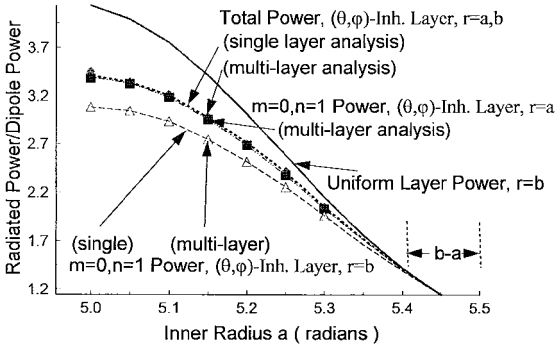

Fig. 3. A comparison of the total normalized powers that occur when the dielectric shell is taken to be a uniform layer (the power, here, is calculated at $r = a, b$ by Bessel-function matching) and when the dielectric shell is taken to be a (θ, φ)-inhomogeneity profile with $\Delta\varepsilon_\theta = 2.8$, $\Delta\varepsilon_\varphi(r) = 0.4$ (Case 2). Here, the power is calculated at $r = a, b$ by a single-layer analysis and a multilayer analysis. The $m = 0, n = 1$ order power is also shown.

[Case 2]. The power here is calculated at $r = a, b$ by a single-layer analysis and a multilayer analysis. As can be seen from Fig. 3, the presence of the (θ, φ)-inhomogeneity profile causes a marked difference in the total scattered power of the inhomogeneous shell, despite the fact that the bulk dielectric inhomogeneity profile was exactly the same as that of the uniform homogeneous shell. It is also noticed from Fig. 3, that for both the single and multilayer analyses, the law of power conservation at $r = a$ and $r = b$ is obeyed to a reasonable degree of accuracy. Also plotted in Fig. 3 is the $m = 0, n = 1$ power at $r = a$. It is noticed that the $m = 0, n = 1(\theta, \varphi)$-inhomogeneity-profile power at $r = a$ almost exactly equals that of the total power at $r = a, b$. This indicates that at $r = a$, no power has been diffracted into higher order modes at the $r = a$ interior boundary shell interface of the system. Fig. 3 also shows the $m = 0, n = 1$ power as calculated at $r = b$. From this plot, one observes that the $m = 0, n = 1$ power is significantly lower than the $r = a, b$ total-power plots. This clearly indicates that as the EM waves have radiated through the dielectric shell, power has been diffracted into the m, n higher order modes of the system. The dielectric shell is acting very much like a planar diffraction grating, which is operating in a transmission mode of operation.

Fig. 4 shows plots of the $n = 2, m = 0$, and $n = 4, m = 0$ mode order power at $r = b$ for the same (θ, φ)-inhomogeneity

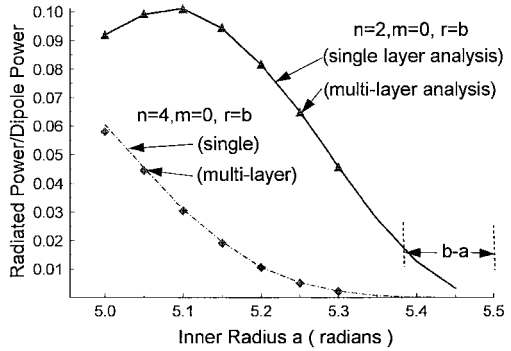

Fig. 4. Plots of the $n = 2,\ m = 0$ and $n = 4,\ m = 0$ mode order power for the same $(\theta,\ \varphi)$-inhomogeneity profile, as was studied in Fig. 3, are shown. The $n = 3,\ 5\ (m = 0)$ orders were very small and not plotted.

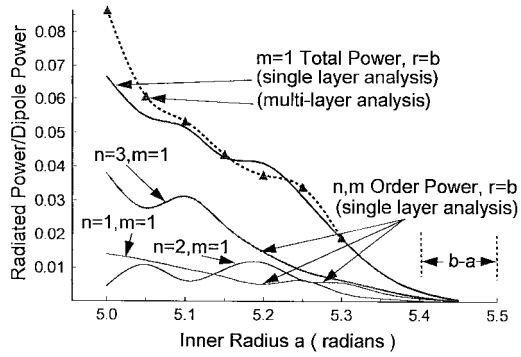

Fig. 5. Plots of the $m = 1$ total power (formed by summing all $m = 1$, $n = 1,\ 2,\ 3,\ \cdots$, mode powers) as computed by using a multilayer analysis (dotted-line triangle) and using a single-layer analysis (solid line) are shown.

profile as was studied in Fig. 3. The $n = 3,\ 5\,(m = 0)$ orders were very small and not plotted. As can be seen from Fig. 4, as the inhomogeneous-shell-thickness $b - a$ is increased, the diffracted power is transferred from the $n = 1,\ m = 0$ lowest order mode (see Fig. 3) to the $n = 2,\ m = 0$ mode, the $n = 4,\ m = 0$ mode and to other higher order modes. One also notices the interesting behavior that at about $a = 5.1$ rad, $b - a = 0.4$ rad, the $n = 2,\ m = 0$ mode power has reached a maximum value and decreases with further increase of the inhomogeneity shell thickness $b - a$. Evidently, the $n = 2,\ m = 0$ higher order mode is, itself, transferring energy to other higher order modes. This behavior is very common in planar diffraction gratings [23].

Fig. 5 shows plots of the $m = 1$ total power (formed by summing all $m = 1$, $n = 1, 2, 3, \cdots$, mode powers) as computed by using a multilayer analysis (dotted-line triangle) and using a single-layer analysis (solid line). One notices that the single and multilayer analyses give approximately the same result up to about a shell thickness of $b - a = 0.4$ rad, but after this value the multilayer analysis is needed for more accurate results. Fig. 5 also shows the $m = 1$, $n = 1,\ 2,\ 3$ order power as calculated by a single-layer analysis. One observes that as the shell thickness $b - a$ increases, the $m = 1$, $n = 1,\ 2,\ 3$ order power increases.

Fig. 6 shows a plot of the total normalized power that results when the $(r,\ \theta,\ \varphi)$-inhomogeneity profile of Case 3 was solved using a multilayer RCWT analysis and using $M_T = 4$ and

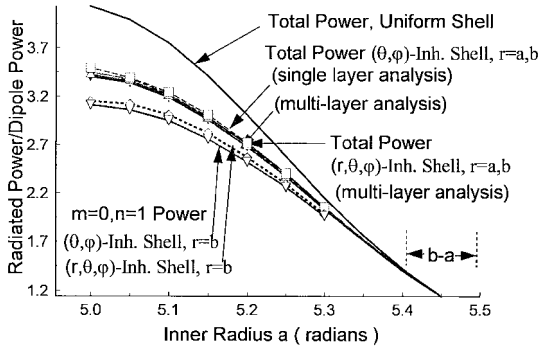

Fig. 6. Plot of the total normalized power that results when the $(r,\ \theta,\ \varphi)$inhomogeneity profile of Case 3 was solved using a multilayer RCWT analysis and using $M_r = 4$ and $I_r = 5$ is shown. Also shown for comparison, is the total power of a uniform shell system (Case 1 parameters) and the total power when a $(\theta,\ \varphi)$ inhomogeneity profile was used with $\Delta\varepsilon_\varphi(r)$ set to a constant value of $\Delta\varepsilon_\varphi(r) = .375$.

$I_T = 5$. Also shown for comparison is the total power of a uniform shell system (Case 1 parameters) and the total power that results when a $(\theta,\ \varphi)$-inhomogeneity profile was used with $\Delta\varepsilon_\varphi(r)$ set to a constant value of $\Delta\varepsilon_\varphi(r) = 0.375$. This value of $\Delta\varepsilon_\varphi(r)$ exactly equaled the average radial value of the $\Delta\varepsilon_\varphi(r)$ function of Case 3 over the interval $a \le r \le b$, $a = 5$ rad and $b = 5.5$ rad. As can be seen from Fig. 6, the $\Delta\varepsilon_\varphi(r)$ linear taper causes little difference in total power to be seen between the total power of the $(r,\ \theta,\ \varphi)$-inhomogeneity profile of Case 3 and the total power of the $(\theta,\ \varphi)$-inhomogeneity profile that used a constant value of $\Delta\varepsilon_\varphi(r) = 0.375$. One notices from Fig. 6 that power conservation was observed to hold to a reasonable degree of accuracy. Fig. 6 also shows a plot of the $m = 0$, $n = 1$ order power calculated at $r = b$ rad for the two inhomogeneity profiles for which the total power was just described. As can be seen from Fig. 6, a perceptible difference in the plots due to the different inhomogeneity profiles is observed.

Fig. 7 shows a $m = 1$ (and $m = 3$) total-order power comparison between the two inhomogeneity profiles discussed in Fig. 6. As can be seen from Fig. 7, at $a = 5$ rad (shell thickness $b - a = 0.5$ rad), the presence of the $\Delta\varepsilon_\varphi(r)$ linear taper for the $(r,\ \theta,\ \varphi)$-inhomogeneity profile of Case 3 causes an observable difference with the $m = 1$ total-order power of the $(\theta,\ \varphi)$-inhomogeneity profile that used a constant value of $\Delta\varepsilon_\varphi(r) = 0.375$ value. As the same multilayer algorithm was used to calculate the $a = 5$ (rad), $m = 1$ total power plots, with the only difference being that a linear and constant $\Delta\varepsilon_\varphi(r)$ function was used, one concludes that completely correct results can only be achieved in the general $(r,\ \theta,\ \varphi)$-inhomogeneity case by using a multilayer analysis.

It is interesting to compare the unit periodic cell formed by the spherical dielectric shell of the present section with the unit cell of a planar crossed-dielectric diffraction grating whose grating dimensions are $\tilde{\Lambda}_x,\ \tilde{\Lambda}_y$. For the spherical system using the inner radius value of $\tilde{r} = \tilde{a}$, the area of the spherical-unit cell is $4\pi\,\tilde{a}^2$. If one chooses $\tilde{\Lambda}_x = \tilde{\Lambda}_y = 2\sqrt{\pi}\tilde{a}$, the grating cell areas of the planar system and spherical one are equal. For the present example, the inner surface of the dielectric shell had $a = k_0\tilde{a} = (2\pi/\lambda)\tilde{a} = 5$ rad, which thus leads

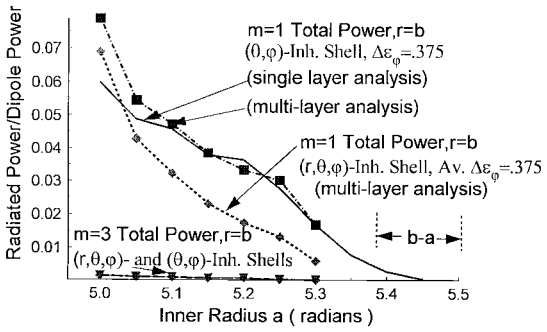

Fig. 7. $m = 1$ (and $m = 3$) total-order power comparison between the two inhomogeneity profiles discussed in Fig. 6.

to $\tilde{\Lambda}_x = \tilde{\Lambda}_y = (5/\sqrt{\pi})\lambda = 2.82\lambda$. It is interesting to note that this grating cell size is very typical of many analyses which are made of planar diffraction gratings. For example, in holographic applications, if two interfering plane waves make an angle of 10.21° on opposite sides of a normal to the holographic surface, a one-dimensional (1-D) diffraction grating of width $\tilde{\Lambda}_x = 2.82\lambda$ is formed. Thus, one sees that diffraction from the spherical-shell system studied in this section is on the same scale size as diffraction that occurs in many planar diffraction analyses. It is also interesting to note that the spherical-shell scattering analysis which was studied in this section would, in the area of diffraction grating theory, be classified as a thin-grating diffraction analysis. This follows as the spherical-shell thickness is less than the grating period and the percent of modulation for the spherical-shell $\Delta\varepsilon_\theta/\varepsilon_2 \cong 2.8/7 = 40\%$, which for planar diffraction grating analysis is large. (Holograms have a depth of modulation on the order of $\approx$ 0.03%.)

IV. Summary and Conclusion

This paper has presented a RCWT analysis of the EM radiation that occurs when a centered electric dipole excites power and energy in a general 3-D inhomogeneous spherical system. The formulation of this paper consisted of a multilayer SV analysis of Maxwell's equations in spherical coordinates (the SV analysis was expressed in terms of spherical EM-field variables) as well as a presentation of the EM fields which bounded on the interior and exterior sides of the inhomogeneous shell. A detailed description of the matrix processing which was involved with finding the final EM fields of the system was given. Three numerical examples of the RCWT method were studied.

It is interesting to compare, for the example solved in Section III, the numerical matrix size required by a method of moments (MoM) algorithm (or finite-element (FE) algorithm) with the numerical size required by the RCWT algorithm used in this paper. For the material shell studied in this paper, the material wavelength is typically $\lambda' = \lambda/\sqrt{(\varepsilon_2 + \Delta\varepsilon_\theta)\mu_2} = \lambda/\sqrt{(9.8)(1.3)} = \lambda/3.56$ free-space wavelengths. The material shell studied had an exterior radius $b = 5.5$ (rad) $= k_0\tilde{b} = (2\pi/\lambda)\tilde{b}$ and, thus, $\tilde{b} = 3.12\lambda'$. The volume of the spherical shell is thus $V_{\text{shell}} = 127.\lambda'^3$. Using the MoM or FE algorithm, volume cells which are $\lambda'/10$ on an edge, requires that 127 000 volume cells be used. Assuming six unknown field variables for each MoM or FE algorithm volume cell, requires 762 000 unknowns for the overall MoM or FE solution. The RCWT algorithm requires that a $(P_T \times P_T)$ matrix equation be solved, where $P_T = 4(2M_T + 1)(2I_T + 1)$. For the example of this paper, $M_T = 4$ and $I_T = 5$ and, thus, a matrix equation involving $P_T = 396$ unknowns was needed to solve the problem. Despite the fact that the RCWT algorithm requires a SV eigen-analysis, the numerical requirements of the RCWT algorithm are still much lower than that of the MoM or FE analysis.

There are several areas of future work for which the theory of this paper may be applied. First, this paper has analyzed scattering from a centered electric-dipole source. The theory of this paper could be used to study plane-wave scattering from an inhomogeneous object, if one expanded an exterior incident plane wave in a Schelkunoff vector potential expansion, as is done to study scattering from a homogeneous dielectric sphere [3, Ch. 6], and then solved the resulting RCWT equations which have already been presented. A second area of research concerns the regions which bound the inhomogeneous region. The present paper has analyzed a spherical inhomogeneous system in the simplest bounding case possible, namely the bounding case when the interior and exterior regions to the inhomogeneous shell are uniform isotropic materials. There is no reason why, for example, the region exterior to the inhomogeneous region couldn't be part of a microwave system (e.g., cavity or waveguide section) or could consist of other scattering objects. In the case of a waveguide section, for example, one would chose waveguide modal fields as the fields exterior to the inhomogeneous region, match EM boundary conditions between the SV field solution and the exterior fields as has already been done in this paper, and then solve the resulting RCWT matrix equations to obtain the overall fields of the system. The multilayer analysis also allows the Region-1 and Region-3 boundaries to be nonspherical surfaces. The problem of a cube of material embedded in a spherical material could be solved by the spherical RCWT algorithm of this paper using the multilayer portion of the algorithm to describe the nonspherical surfaces of the cube. A third area of research would be to extend the SV analysis of (2)–(5) to apply to an anisotropic material region. This problem of determining the EM fields of an anisotropic planar diffraction grating has already been studied with great success in [20]. There is no reason why a similar analysis cannot be made for the present spherical system. A fourth area of research would be to implement the RCWT algorithm on a high-performance massively parallel computer. Using the multilayer analysis, one could solve the SV equations of each thin layer simultaneously on a parallel machine and, thus, achieve rapid solution of the overall EM scattering problem. Good load balance can be anticipated since the same-size SV analysis would be performed in each layer. It is finally noted that the RCWT algorithm has been widely studied in its application to planar diffraction gratings ([20] has an extensive reference list) and should be widely available to those who would like to use it.

REFERENCES

[1] J. R. Wait, *Electromagnetic Radiation from Cylindrical Structures.* New York: Pergamon, 1959.

[2] H. Y. Yee, "Scattering of electromagnetic waves by circular dielectric coated conducting cylinders with arbitrary cross sections," *IEEE Trans. Antennas Propagat.,* vol. AP-13, pp. 822–823, 1965.

[3] R. F. Harrington, *Time-Harmonic Electromagnetic Fields.* New York: McGraw-Hill, 1961.

[4] C. A. Balanis, *Advanced Engineering Electromagnetics.* New York: Wiley, 1989.

[5] P. Bhartia, L. Shafai, and M. Hamid, "Scattering by an imperfectly conducting conductor with a radially inhomogeneous dielectric coating," *Int. J. Electron.,* vol. 31, pp. 531–535, 1971.

[6] A. A. Kishk, R. P. Parrikar, and A. Z. Elsherbeni, "Electromagnetic scattering from an eccentric multilayered circular cylinder," *IEEE Trans. Antennas Propagat.,* vol. 40, pp. 295–303, Mar. 1992.

[7] X. B. Wu, "Scattering from an anisotropic cylindrical dielectric shell," *Int. J. Infrared Millimeter Waves,* vol. 15, no. 10, pp. 1733–1743, 1994.

[8] ———, "An alternative solution of the scattering from an anisotropic cylindrical dielectric shell," *Int. Infrared Millimeter Waves,* vol. 15, no. 10, pp. 1745–1754, 1994.

[9] W. Ren, "Contributions to the electromagnetic wave theory of bounded homogeneous anisotropic media," *Amer. Physical Soc., Physical Rev. E,* vol. 47, no. 1, pp. 664–673, Jan. 1993.

[10] A. Z. Elsherbeni and M. Hamid, "Scattering by a cylindrical dielectric shell with inhomogeneous permittivity profile," *Int. J. Electron.,* vol. 58, no. 6, pp. 949–962.

[11] ———, "Scattering by a cylindrical dielectric shell with radial and azimuthal permittivity profiles," in *Proc. 1985 Symp. Microwave Technol. in Ind. Develop.,* Brazil, July 22–25, 1985, pp. 77–80 (invited paper).

[12] A. Z. Elsherbeni and M. Tew, "Electromagnetic scattering from a circular cylinder of homogeneous dielectric coated by a dielectric shell with a permittivity profile in the radial and azimuthal directions—Even TM case," in *Proc.—1990 Southeastcon'90,* New Orleans, LA, Apr. 1–4, 1990, session 11A-1, pp. 996–1001.

[13] J. M. Jarem, "Rigorous coupled wave theory solution of phi-periodic circular cylindrical dielectric systems," *J. Electromagnetic Waves and Applications,* vol. 11, pp. 197–213, 1997.

[14] M. G. Moharam and T. k. Gaylord, "Rigorous coupled-wave analysis of grating diffraction-E-mode polarization and losses," *J. Opt. Soc. Amer.,* vol. 73, no. 4, pp. 451–455, Apr. 1983.

[15] ———, "Rigorous coupled-wave analysis of planar grating diffraction," *J. Opt. Soc. Amer.,* vol. 71, no. 7, pp. 811–818, 1981.

[16] K. Rokushima and J. Yamakita, "Analysis of anisotropic dielectric gratings," *J. Opt. Soc. Amer.,* vol. 73, pp. 901–908, 1983.

[17] M. G. Moharam and T. K. Gaylord, "Three-dimensional vector coupled-wave analysis of planar-grating diffraction," *J. Opt. Soc. Amer.,* vol. 73, pp. 1105–112, 1983.

[18] ———, "Diffraction analysis of dielectric surface-relief gratings," *J. Opt. Soc. Amer.,* vol. 72, pp. 1385–1392, 1987.

[19] M. G. Moharam, "Coupled-wave analysis of two-dimensional dielectric gratings," *Holographic Optics: Design and Applications,* vol. SPIE-883, pp. 8–11, 1988.

[20] E. N. Glytsis and T. K. Gaylord, "Rigorous three-dimensional coupled-wave diffraction analysis of single cascaded anisotropic gratings," *J. Opt. Soc. Amer. A,* no. 11, vol. 4, pp. 2061–2080, 1987.

[21] J. M. Jarem, "A rigorous coupled wave theory and crossed diffraction grating analysis of radiation and scattering from three-dimensional inhomogeneous objects," *IEEE Trans. Antennas Propagat.,* submitted for publication.

[22] M. Abramowitz and I. Stegum, *Handbook of Mathematical Functions.* ———NY: Dover, 1972, p. 360, eq. 9.1.20.

[23] J. M. Jarem and P. Banerjee, "An exact, dynamical analysis of the Kukhtarev equations in photorefractive barium titanate using rigorous wave coupled wave diffraction theory," *J. Opt. Soc. Amer. A,* vol. 13, no. 4, pp. 819–831, Apr. 1996.

John M. Jarem, (M'82–SM'97) received the BSEE, MSEE, and Ph.D. degrees from Drexel University, Philadelphia, PA, in 1971, 1972, and 1975, respectively.

From 1975 to 1981, he worked as an Assistant Professor and Associate Professor at the University of Petroleum and Minerals, Dhahran, Saudi Arabia. From 1981 to 1987, he was a Professor of electrical engineering and computer engineering at the University of Alabama, Huntsville. His research interests are electromagnetics and antenna theory.